Polar Science 27 (2021) 100599

Contents lists available at ScienceDirect

Polar Science

journal homepage: http://www.elsevier.com/locate/polar

Increasing dust emission from ice free terrain in southeastern Greenland since 2000

Tomomi Amino[a,b,1], Yoshinori Iizuka[a,*], Sumito Matoba[a], Rigen Shimada[c], Naga Oshima[d], Toshitaka Suzuki[e], Takuto Ando[f], Teruo Aoki[g], Koji Fujita[h,**]

[a] Institute of Low Temperature Science, Hokkaido University, Kita 19-jo Nishi 8-chome, Kita-ku, Sapporo, 060-0819, Japan
[b] Graduate School of Environmental Science, Hokkaido University, Kita 10-jo Nishi 5-chome, Kita-ku, Sapporo, 060-0810, Japan
[c] Earth Observation Research Center, Japan Aerospace Exploration Agency, 2-1-1, Sengen, Tsukuba, Ibaraki 305-8505, Japan
[d] Meteorological Research Institute, 1-1 Nagamine, Tsukuba, Ibaraki 305-0052, Japan
[e] Faculty of Science, Yamagata University, 1-4-12 Kojirakawa, Yamagata 990-8560, Japan
[f] Arctic Research Center, Hokkaido University, Kita 21-jo Nishi 11-chome, Kita-ku, Sapporo, 060-0819, Japan
[g] National Institute of Polar Research, 10-3, Midori-cho, Tachikawa-shi, Tokyo 190-8518, Japan
[h] Graduate School of Environmental Studies, Nagoya University, F3-1(200) Furo-cho, Chikusa-ku, Nagoya 464-8601, Japan

ARTICLE INFO

Keywords:
Greenland
Dust
Ice core
Annual flux
Seasonal flux

ABSTRACT

Mineral dust plays a key role in both local and global climates. At high latitudes, atmospheric dust can affect ice-nuclei formation, and surface dust can reduce the albedo as well as increase subsequent ice melting. As a proxy for past climate, mineral dust is preserved in ice cores, but few studies have examined deposited dust in ice cores during the Anthropocene, especially after 2000. We measured dust concentrations in an ice core at the southeastern dome in Greenland (SE-Dome), and reconstructed the annual and seasonal dust fluxes during 1960–2014. We find the annual average flux during 1960–2014 to be 34.8 ± 13.5 mg m^{-2} yr^{-1}, a value about twice that of ice cores further inland. The more recent part of that period, 2000–2014, has the higher annual flux of 46.6 ± 16.2 mg m^{-2} yr^{-1}. The annual and autumn dust fluxes highly correlate with air temperature in Tasiilaq ($r = 0.61$ and 0.50, respectively), a coastal location in southeastern Greenland. Our results suggest that the local dust emissions at the coastal region are increasing due to a decreasing seasonal snow-cover area arising from coastal Greenland warming after 2000.

1. Introduction

Mineral dust has global and local effects on climate (Carslaw et al., 2010; Kok et al., 2018). Globally, mineral dust can directly influence the atmospheric radiation budget and indirectly affect the radiation budget via the cloud condensation nucleus effect (e.g., Stanelle et al., 2014). Locally, mineral dust is known to affect hot, arid, and subtropical regions (e.g., Mahowald et al., 2006, 2014). However, it is increasingly recognized that dust produced at high latitudes and cold environments mflay extend beyond the local source area and have regional, and even global, significance (Bullard et al., 2016).

The motion of glaciers produces fine sediment (glacial flour) that is delivered via meltwater to proglacial floodplains. Then, when the glacier retreats, more land surface area with fine sediment becomes exposed to wind action, meaning that local dust emissions at high latitudes are likely to increase in a warming climate (Bullard, 2013; Simonsen et al., 2019). Once airborne, such glacial-outwash dust has a remarkably high ice-nucleating ability under conditions relevant for mixed-phase cloud formation (Tobo et al., 2019). In addition, at high latitudes, the low humidity, strong winds, permafrost, and niveo-aeolian processes promote dust emission and distribution of sediments. The subsequent dust deposition on the surface of ice sheets and glaciers can decrease ice albedo and increase subsequent glacier melting (e.g., Aoki et al., 2006; Fujita, 2007; Fujita et al., 2011; Nagorski et al., 2019).

Ice cores drilled in high-latitude regions preserve past aerosols including mineral dust (e.g., Lambert et al., 2008). The source of the

* Corresponding author.
** Corresponding author.
E-mail addresses: iizuka@lowtem.hokudai.ac.jp (Y. Iizuka), cozy@nagoya-u.jp (K. Fujita).
[1] present address: ORGANO Corporation, 1-2-8 Shinsuna, Koto-ku, Tokyo, 136–8631, Japan.

https://doi.org/10.1016/j.polar.2020.100599
Received 12 March 2020; Received in revised form 28 September 2020; Accepted 28 September 2020
Available online 3 October 2020
1873-9652/

mineral dust has been studied mainly by using the isotopic method (Bory et al., 2003; Delmonte et al., 2008). Over the long term, mineral dust contributes to the glacial–interglacial cycle as a cooling factor (e.g., Seinfeld and Pandis, 1998). Dust deposited in inland Greenland mostly consists of the fine grain size (<5 μm), mainly coming from long-term transport from Asian source regions (Biscaye et al., 1997; Bory et al., 2002; Bory et al., 2003; Uno et al., 2009). On the other hand, dust deposited on the Renland ice cap, a coastal region in Greenland, is dominated by coarse particles (>5 μm), suggesting a dust source local to the ice cap that sediments rapidly, typically within one day (Simonsen et al., 2019). Other regions on the Greenland ice sheet that may have significant contributions from both long-transported Asian and short-transported local sources have not been examined in detail.

Over the local scale and short-term, the picture is less clear. Few studies of deposited dust in ice cores of inland Greenland have covered the Anthropocene, especially after 2000. From a lake-sediment core in west Greenland, Saros et al. (2019) found that after 2006, the mean July air temperature shifted 1.1 °C higher. They also found that nonlinear environmental responses occurred with or shortly after the abrupt climate shift, including increases in both dust and ice-sheet discharge. However, the dating uncertainty of ice cores makes it difficult to compare an ice-core proxy such as dust with a climatic index such as air temperature. Over the past 600 years, the warmest period began after 2000. The dust in this period has been modeled and monitored by satellite, but such approaches have been insufficient for understanding local-scale climate systems (Bullard et al., 2016). For example, satellite detection of dust is particularly challenging in the high latitudes due to darkness above the polar circles in late fall and winter (Bullard et al., 2016). Thus, a record of deposited dust from an ice core with accurate dating resolution would greatly help us evaluate the relationship between dust and the local climate system.

The Greenland ice sheet has a dome in the southeastern area (SE-Dome; 67.18°N, 36.37°W, 3170 m a.s.l.), located on the margin of Greenland ice sheet. Despite its high altitude of over 3000 m a.s.l., the SE-Dome is located near the North Atlantic Ocean. The SE-Dome lies midway between ice-core sites in inland Greenland and Renland. Thus, the SE-Dome is an ideal location to evaluate contributions of both Asian and local sources of mineral dust. Also, due to the extremely high accumulation rate at the SE-Dome, its ice-core record has a high time resolution (Iizuka et al., 2017). Calibration between oxygen isotope ($\delta^{18}O$) data from SE-Dome samples and $\delta^{18}O$ models produced a reconstruction of the paleoclimate and atmospheric circulation over the last 60 years with an uncertainty of ±2 months (Furukawa et al., 2017). Thus, over this period, paleoclimate reconstruction here allows one to examine the relationship between dust and climate on the seasonal scale. In this study, we analyzed dust concentrations in the SE-Dome ice

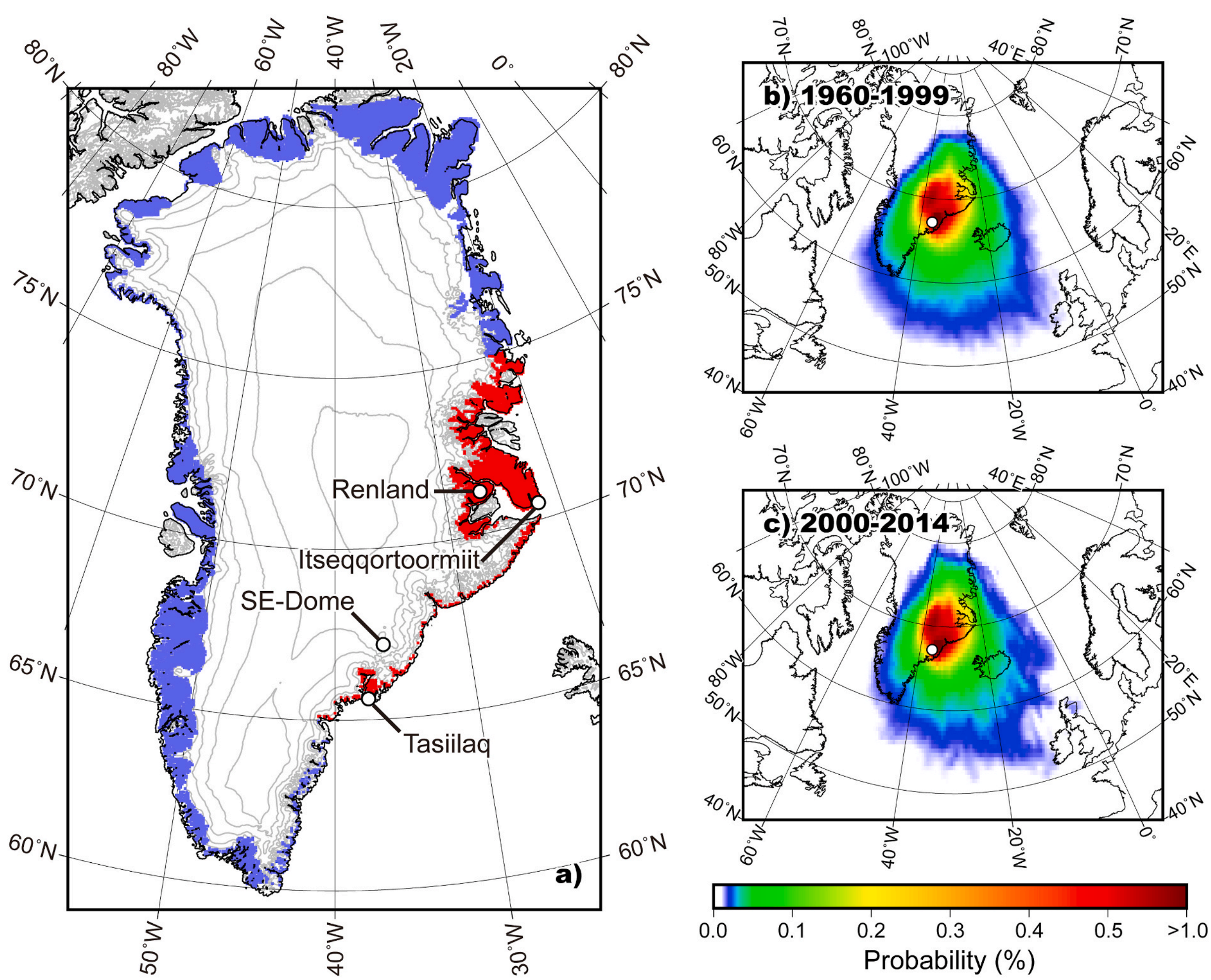

Fig. 1. Study area and air-mass trajectories. (**a**) Locations of southeast dome (SE-Dome), Tasiilaq, Itseqqortoormiit, and Renland. Blue and red shaded regions denote potential snow-free areas bordering the Greenland Ice Sheet. The red regions are obtained from the air-mass trajectories in Fig. 1b and c (east coast between 65 and 75 °N), and used to calculate snow-free area in September (Fig. 2c). (**b**) Probability distribution (%) of an air mass arriving at the SE-Dome site from a 3-day, 3-D backward-trajectory analysis, averaged over 1960–1999 for air-mass starting elevations 10 and 500 m a.g.l. Color scale at bottom. **(c)** Same as (b) except for period 2000–2014. Probability of the air mass is weighted by the daily precipitation from combined reanalysis datasets of ERA-40 and ERA-Interim. (For interpretation of the references to colour in this figure legend, the reader is referred to the Web version of this article.)

core over this period, investigating the relationship between the climate system and a high-latitude dust source, with focus on the post-2000 years.

2. Materials and methods

2.1. SE-dome ice core and age scale

Dust data came from a 90.45-m depth ice core obtained at a dome site on the SE-Dome (67.18°N, 36.37°W, 3170 m a.s.l., Fig. 1a). The annual mean temperature at the SE-Dome is −20.9 °C, based on 20-m-deep firn-temperature measurements (Iizuka et al., 2017). For a time-scale, we use the SEIS2016 age scale for 1960–2014, which is determined by the oxygen-isotope matching method (Furukawa et al., 2017). The SEIS2016 scale has been carefully evaluated with independent age markers of tritium and volcanic events, and its precision is within two months (Fig. 3 in Furukawa et al., 2017). Depths marking the beginning of the year are found by linear interpolation.

2.2. Microparticle (dust) concentration measurements

In a cold room (Institute of Low Temperature Science, Hokkaido University, Japan), we divided the 90.45-m ice core into 941 sections, each of close to 100 mm depth. Based on the SEIS2016 age scale, uppermost 852 samples cover the period from 1960 to 2014. The samples were divided using a clean ceramic knife in a cold clean room (class 10000), put into clean polyethylene bottles, and then were melted in the bottle at room temperature in a clean room. Concentration and grain-size distributions of the microparticles, hereafter dust, were measured using a Beckman Coulter Counter Multisizer 3 with an aperture of 30 μm (size range between 0.6 and 18 μm in diameter) in a class 10000 clean room.

To make a measurement solution of 15 ml, we mixed 3 ml of melted ice-core sample with 12 ml of a liquid dilution agent (ISOTON II, Beckman) in a 25 ml bottle (Accuvette ST, Beckman). To dissolve any bubbles in the melted water, the solutions were kept at least 24 h in the clean room after melting. Then, to homogenize the settled (larger) particles, the solutions were gently stirred using a 1000 μl pipette (Eppendorf Research) without making bubbles. For the background value, we ran a blank test of the above method by using 96 samples with

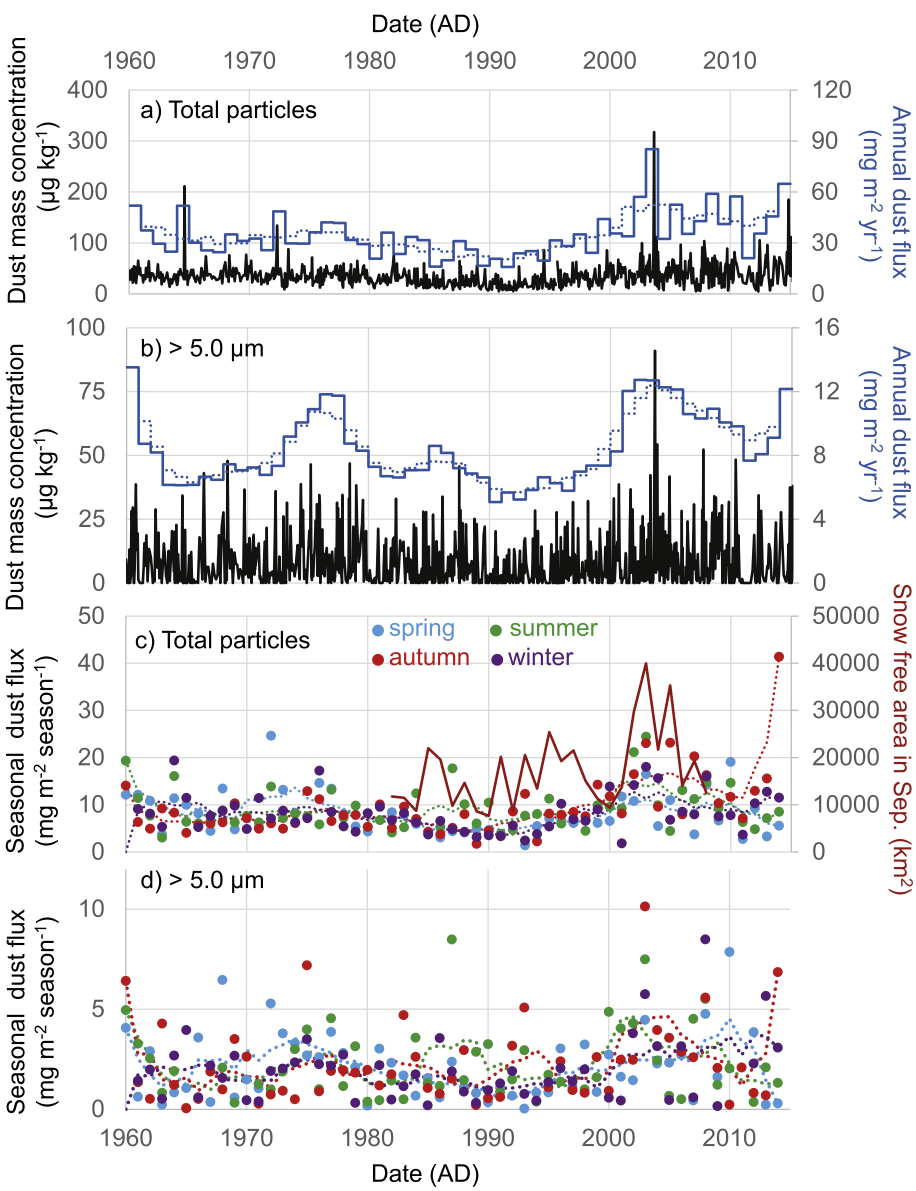

Fig. 2. Trends in dust mass, dust flux, and snow-free coastal area. **(a)** Annual dust mass concentration (left) and dust flux (right) in the SE-Dome ice core. Dotted line shows a running average over 5 years. **(b)** Same as (a) except for particles exceeding 5 μm. **(c)** At left are seasonal dust fluxes in the SE-Dome ice core. Blue, green, red, and purple for spring, summer, autumn, and winter, respectively, the dotted lines are running averages over 5 years. At right, snow-free area in September on the east coast of Greenland within 65–75°N derived from AVHRR from 1979 to 2008. (Data losses in 1980 and 1981 are due to having insufficient satellite observations for that period.) **(d)** Same as (c) except for particles exceeding 5 μm and without the snow-free area. (For interpretation of the references to colour in this figure legend, the reader is referred to the Web version of this article.)

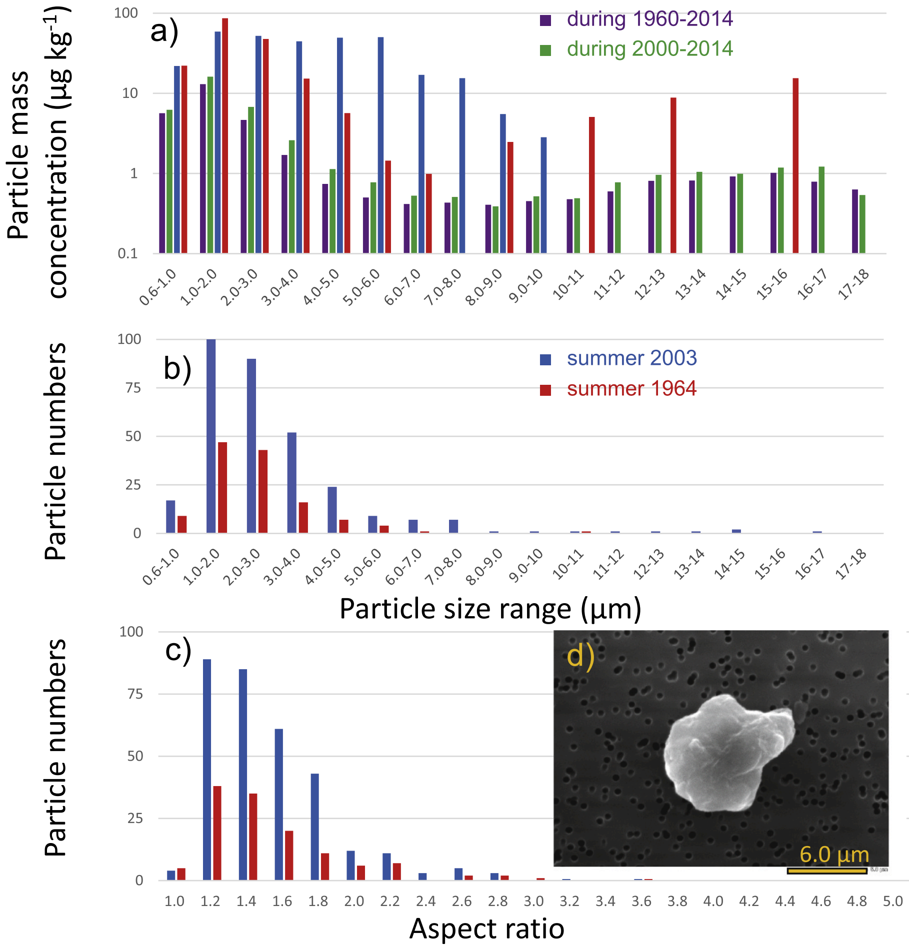

Fig. 3. Particle distributions. **(a)** Particle mass–size distribution by the Colter Counter method during 1960–2014 (purple), 2000–2014 (green), summer 1964 (red) and summer 2003 (blue). (**b**) Particle number–size distribution by the SEM method on summer 1964 (red) and summer 2003 (blue). **(c)** Same as (b) except for particles' aspect ratio. (**d**) Example of a particle larger than 5 μm from summer 2003. (For interpretation of the references to colour in this figure legend, the reader is referred to the Web version of this article.)

ultra-pure water (18.2 MΩ cm). Each sample consisted of 3 ml of the ultra-pure water and 12 ml of the diluent. The average and standard deviation of the particle number and mass concentration were 1900 ± 423 ml^{-1} and 2.6 ± 1.0 μg kg^{-1}, respectively. The mass concentration was calculated from dust volumes, assuming a spherical approximation and a density of 2.50 g cm^{-3}.

2.3. Flux estimation

The annual and seasonal dust fluxes are based on the seasonal average value of each dust concentration value multiplied by the seasonal accumulation rate. The seasonal boundaries are March 1st, June 1st, September 1st, and December 1st for spring (MAM), summer (JJA), autumn (SON), and winter (DJF). The annual dust fluxes use the boundary of January 1st. These annual and seasonal accumulation rates are estimated based on the SEIS2016 age scale (Furukawa et al., 2017).

2.4. Observation of particle sizes and shapes

Insoluble particles were collected on a polycarbonate membrane filter (Advantec 13 mm, pore size 0.4 μm) following the method in Iizuka et al. (2009). The filter was coated with Pt by using magnetron sputter (MSP-10, Vacuum Device). Then, the particle shape was observed using a scanning electron microscope (JSM-6360LV, JEOL) with an energy dispersive x-ray spectrometer (JED2201, JEOL). We confirmed that almost all measured particles contained Si, indicating silicate minerals (dust). To determine their shapes, we examined particles in a sample from summer 1964 (depth 80.105 m) and a sample from summer 2003 (24.800 m), which had the largest dust mass concentrations in 1960–1999 and in 2000–2014, respectively.

2.5. ERA-40 and ERA-Interim reanalysis data

To evaluate climate records in the SE-Dome ice core, we used the ERA-40 (1958–2001) and ERA-Interim (1979–2014), hereafter ERA-I, reanalysis datasets produced by the European Centre for Medium-Range Weather Forecasts (ECMWF) (Uppala et al., 2005; Dee et al., 2011). The daily and monthly mean air temperature at the SE-Dome elevation (3170 m a.s.l.) were extracted from the pressure level air temperature by referring to the geopotential height, both in ERA-40 and ERA-I (Sakai et al., 2015; Furukawa et al., 2017). Daily precipitation was also retrieved from ERA-40 and ERA-I for the backward trajectory analysis. To maintain consistency between the two precipitation products for the whole period (1958–2014), the daily precipitation of ERA-40 (p_{40}) is calibrated with that of ERA-Interim (p_I) by a linear regression obtained for the period 1979–2001 ($p_I = 1.36p_{40}, R^2 = 0.862$, $p < 0.001$, Iizuka et al., 2018).

2.6. Backward trajectory analysis

To investigate source regions of the chemical species in the ice core, transport pathways of air masses are analyzed using the HYSPLIT model (hybrid single-particle Lagrangian integrated trajectory), a model distributed by NOAA (National Oceanographic and Atmospheric Administration) (Stein et al., 2015). We followed the backward trajectory analysis as described in Iizuka et al. (2018), and set four points at 10, 500, 1000, and 1500 m above ground level (a.g.l.) at SE-Dome for the start of the three-day backward trajectory calculation.

2.7. Remotely sensed snow-free terrain

To investigate how variations in the distribution of snow-free areas affect dust sources during 1979–2008, we used a 0.05° gridded daily calibrated radiance and classification product derived from the Advanced Very High Resolution Radiometer (AVHRR). Details of this product are in Hori et al. (2017). Product flag values are defined as snow, sea ice, bare land, open ocean, and cloud. To calibrate the snow-free pixels, we used the bare land flags on the Greenland region defined by DiMarzio (2007). Over a month, we counted the number of days a given pixel was flagged as "bare land" and the number of days it was not flagged as "cloud", then took the ratio. If the ratio exceeded 0.5, it was classified "snow-free" for the month. This procedure was done for each pixel of the designated area for the months from April to September. The extracted snow-free pixels were projected onto Lambert's azimuthal equal-area projection to calculate the areal extent. The month with maximum snow-free area (July or August) is defined as the "maximum month". For the analysis, the designated area was that within 65–75 °N of the east coast of Greenland (Fig. 1), the most likely source region of local dust based on the backward trajectory analysis (maximum area of 6.5×10^4 km^2).

3. Results and discussion

3.1. Dust concentrations

The average concentration of dust particle number in the SE-Dome ice core over 1960–2014 is 13000 ± 6200 ml^{-1} (Table 1). (Unless otherwise noted, uncertainties here are the standard deviation.) The numbers also show that the concentration during 2000–2014 is 14800 ± 6880 ml^{-1}, which is almost same or slightly higher than that over 1960–2014. Larger particles (over 5 μm) are smaller in number, but show the same trend, almost same or slightly increasing from 9.08 ± 1.43 ml^{-1} for 1960–2014 to 11.5 ± 2.32 ml^{-1} for 2000–2014.

From the profile in Fig. 2a, the dust mass concentration has an average value (1960–2014) of 34.2 ± 22.1 μg kg^{-1}. The average blank error is 7.6% in this study. Table 1 shows that the average mass concentration increases after 2000 to 42.9 ± 29.1 μg kg^{-1}. Both are within 1σ, but the mass concentration is 25.4% higher after 2000, but the number concentration is only 13.8% higher. The difference is related to the relative increase of the fraction of coarser particles.

The dust size distribution by mass (green and purple in Fig. 3a) over 1960–2014 show a bimodal trend. One peak occurs around 1–2 μm, the other around 15 μm, suggesting contributions from two sources. The dust size distribution of Renland ice core (the RECAP Holocene) has a peak around 20 μm, suggesting high contribution from local source (Simonsen et al., 2019). Thus, the large particle mode (around 15 μm) of the SE-Dome ice core implies a nearby dust source. As the long-term transport from Asian source regions has particles mostly less than 5 μm (Biscaye et al., 1997; A.-M. Bory et al., 2002; A. J. M. Bory et al., 2003; Uno et al., 2009), we divide the two sources at 5 μm. The mass concentration for dust larger than 5 μm is 10.7 ± 10.8 μg kg^{-1}, which is 31.3% of the total mass concentration during 1960–2014. For the period 2000–2014, the corresponding mass for dust larger than 5 μm is 12.6 ± 12.9 μg kg^{-1}, which is 29.4% of the total mass concentration. Thus, the size distribution by mass shows a similar bimodal trend between 1960–2014 and 2000–2014, suggesting little change of the source (Asian or local) contributions between the two periods. The periods of dust events in summers 1964 and 2003 (red and blue in Fig. 3a) have larger size distributions than those in averaged distribution (green and purple in Fig. 3), suggesting high contribution from local source during the periods.

We examined SEM micrographs of particles from summer 1964 (depth 80.105 m) and summer 2003 (24.800 m). In Fig. 2a, these years have the largest dust mass concentrations in 1960–1999 and in 2000–2014. These seasons did not have any large volcanic eruption in Iceland. The SEM analyses show that the SE-Dome ice core has a significant number of dust particles over 5 μm, especially in 2003 (e.g., Fig. 3d); however, the size distributions have similar trends for summer 1964 and summer 2003 (Fig. 3b). In addition, the dust-particle shapes, as indicated by the aspect ratios, are similar between summer 1964 and summer 2003 (Fig. 3c). The similar size distributions and aspect trends suggests the same contributions from each source region between the two seasons.

3.2. Annual and seasonal dust flux reconstructions

The annual and seasonal dust fluxes equal the product of the mass concentration with their respective accumulation rate (Furukawa et al., 2017). The resulting annual flux for 1960–2014 in Fig. 2a gives an average of 34.8 ± 13.5 mg m^{-2} yr^{-1}. This average is greater than the yearly values of 14–19 mg m^{-2} yr^{-1} at the inland ice cores of GRIP, NGRIP, and Dye3 (Bory et al., 2003), but is less than the 57 mg m^{-2} yr^{-1} at Haus Tausen in the coastal region of north Greenland (Bory et al., 2003) and much less than the 680 mg m^{-2} yr^{-1} at Renland on an ice cap near the ice sheet (Bory et al., 2003). Over the extensive inland region of Greenland, the flux values are low and nearly uniform due to the long-distant transport over high-elevations to the ice sheet (Bory et al.,

Table 2
Seasonal average dust fluxes (mg m^2 season^{-1}) with standard deviations during 1960–1999 and 2000–2014 in the cases of within 0.6–18 μm, and 5.0–18 μm.

Period	Term	Particle size within 0.6–18 μm	Particle size within 5.0–18 μm
1960–1999	Spring	7.79 ± 4.20	2.24 ± 1.47
	Summer	8.24 ± 3.74	2.45 ± 1.71
	Autumn	7.19 ± 2.96	2.38 ± 1.89
	Winter	7.28 ± 3.44	2.21 ± 1.85
2000–2014	Spring	9.01 ± 4.73	2.86 ± 1.81
	Summer	11.2 ± 5.46	3.34 ± 2.42
	Autumn	15.7 ± 8.51	3.72 ± 2.27
	Winter	10.4 ± 4.52	3.06 ± 2.02

Table 1
Average values and standard deviations of number and mass dust concentrations during 1960–2014, 2000–2014, and seasons with large volcano eruption events in Iceland. The average values and standard deviations are shown in the cases of within 0.6–18 μm, and 5.0–18 μm. Seasons with 7 large volcano eruption events in Iceland: 1) Bárðarbunga, autumn 2014; 2) Grímsfjall, spring 2011; 3) Eyjafjallajökull, spring 2010; 4) Hekla, winter 2000; 5) Krafla, autumn 1984; 6) Eldfell, winter 1973; and 7) Askja, autumn 1961.

Term	Particle size (μm)	Number conc.(mL-1)	Mass conc. (μg kg-1)
Period 1960–2014 (n = 850)	0.6–18	13000 ± 6000	34.2 ± 22.1
Period 1960–2014 (n = 850)	5.0–18	9.08 ± 1.43	10.7 ± 10.8
Period 2000–2014 (n = 259)	0.6–18	14800 ± 6880	42.9 ± 29.1
Period 2000–2014 (n = 259)	5.0–18	11.5 ± 2.32	12.6 ± 12.9
Volcanic seasons* (n = 26)	0.6–18	13700 ± 8270	40.1 ± 34.6
Volcanic seasons* (n = 26)	5.0–18	16.4 ± 2.82	14.8 ± 14.9

Table 3
Annual and seasonal correlation coefficients (r) between dust fluxes and potentially relevant proxies during 1960–2014. Bold marks values of 0.5 or higher.

	Ca^{2+}	d^{18}O (‰)	d-excess (‰)	NAO index	AO index	SE-Dome air temperature (°C)	Tasiilaq air tempature (°C)	Itseqqortoormiit air tempature (°C)	Tasiilaq precipitaion (mm)	Itseqqortoormiit precipitaion (mm)	Tasiilaq wind speed (m s^{-1}) [1974–2014]	Snow-free area (km^2) in [a]maximum month [1979–2008]	Snow-free area (km^2) in September [1979–2008]
Refences	Iizuka et al., (2018)	Furukawa et al., (2017)	Furukawa et al., (2017)	Hurrell et al., (2003)	Higgins et al., (2001)	Uppala et al. (2005); Dee et al. (2011)	Cappelen, (2016)	Cappelen, (2016)	Cappelen, (2016)	Cappelen, (2016)	NCEI, NOAA, U. S.	This study	This study
annual [1960–2014]	**0.66**	0.27	−0.07	−0.25	−0.17	0.43	**0.61**	0.35	0.17	0.13	0.41	0.43	**0.58**
spring [1960–2014]	0.37	0.11	−0.03	−0.30	−0.05	0.39	0.20	−0.12	0.25	0.09	−0.12	0.34	0.38
summer [1960–2014]	**0.52**	0.04	−0.12	−0.03	−0.12	0.25	0.38	0.18	−0.06	−0.09	−0.16	0.25	0.30
autumn [1960–2014]	**0.83**	0.20	0.00	−0.02	−0.13	0.20	**0.50**	0.44	−0.09	0.27	0.38	0.49	**0.60**
autumn [1960–2013]	**0.65**	0.32	−0.02	−0.10	−0.05	0.22	**0.52**	0.40	−0.09	0.06	0.46	0.49	**0.60**
winter [1960–2014]	0.17	0.10	0.15	−0.17	−0.27	0.27	0.13	0.09	0.07	0.04	−0.11	0.35	0.38

[a] Maximum month means July or August with greatest snow-free area.

2003). On the other hand, the high dust fluxes in Haus Tausen and Renland are mainly due to the local source (Simonsen et al., 2019). The average flux value of 34.8 mg m^{-2} yr^{-1} of the SE-Dome ice core is about twice that of the inland ice cores. We argue next that this difference indicates that some dust particles come from local sources such as exposed glacial sediments, moraines, rock, soil, and sand in coastal Greenland (e.g. Bullard et al., 2016).

The high contribution to the flux from large particles is one argument for a local dust source. The average annual flux from particles larger than 5 μm is 10.6 ± 4.26 mg m^{-2} yr^{-1} (Fig. 2b, blue curve), which is 30.5% of the total flux value. Due to the relatively rapid fallout of such large particles, they must be from a nearby source. For particles smaller than 5 μm, the average annual flux is the remaining 24.2 (= 34.8 − 10.6) mg m^{-2} yr^{-1}. Of this flux, some must also be from the local sources. The similar method of the 5 μm threshold of dust size dividing long and local transportation was done in coastal Antarctica (Baccolo et al., 2018). If we assume that this remaining dust flux equals that from long distance sources plus fine dust from local sources, with the former equaling that reaching the inland ice cores of GRIP, NGRIP, and Dye3 (14–19 mg m^{-2} yr^{-1}), then the annual flux of fine particles from local sources equals 5.2–10.2 mg m^{-2} yr^{-1}. This amount from local sources is 15.0–29.3% of the total flux. Totaling both the smaller and larger dust flux from the local sources, we estimate that 45.5–59.8% of the dust at the SE-Dome ice core is from a local source.

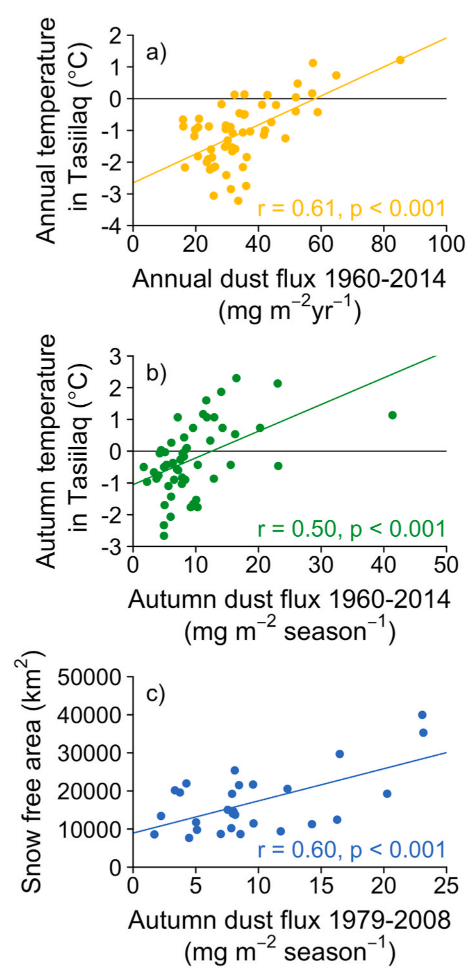

Fig. 4. Correlations of dust fluxes to temperature in Tasiilaq and coastal snow-free area. **(a)** Annual dust flux and annual air temperature at Tasiilaq. **(b)** Autumn dust flux and autumn air temperature at Tasiilaq. **(c)** Autumn dust flux and the snow-free area in September during 1979–2008. Monthly air temperatures 1960–2014 at Tasiilaq (65.60°N, 37.59°W) are from the Danish Meteorological Institute (Cappelen, 2016).

A second argument for a local source contribution comes from the recent trend in annual flux. In particular, the total flux is higher after 2000 (46.6 ± 16.2 mg m^{-2} yr^{-1} during 2000–2014; Table 1 and Fig. 2a), but the flux from Asia is not likely to have increased during this time. In particular, Liu et al. (2020) found that the Asian dust intensity during 1961–2020 was high until 1980 and then decreased to the present (2020). This fact suggests that the Asian dust source by itself cannot explain the high flux after 2000 in the SE-Dome ice core. Given that the atmospheric circulation does not change after 2000 (Fig. 1b and c), the increase after 2000 must be from a local source. In addition, the annual flux of the larger (>5 μm) particles also increased after 2000 to 13.3 ± 5.33 mg m^{-2} yr^{-1} (2000–2014; Table 1 and Fig. 2b). Thus, the contribution from local sources probably increased after 2000.

Finally, a third argument for a local source comes from the trend in seasonal flux. The seasonal fluxes during 1960–2014 are plotted in Fig. 2c. We split this period into before and after 2000. Table 2 shows the averages in both periods. During 1960–1999, the averages are nearly the same for all seasons (7.19–8.24 mg m^{-2} yr^{-1}). For 2000–2014, the highest average is in autumn at 15.7 ± 8.81 mg m^{-2} yr^{-1}, suggesting that the high dust flux after 2000 was mainly driven by the increase in autumn. A similar increase in autumn flux occurs for the large particles (Fig. 2d, Table 2). In particular, the average fluxes during 1960–1999 are nearly the same for all seasons (2.21–2.45 mg m^{-2} yr^{-1}). But for 2000–2014, the highest average is in autumn at 3.72 ± 2.27 mg m^{-2} yr^{-1}. However, Asian dust storms tend to come in spring (e.g., Liu et al., 2020), and thus the increase in autumn flux is more likely due to a local source. In the next section, we suggest a cause of the increasing annual and autumn dust fluxes during 2000–2014.

3.3. Cause of the increase in annual and autumn flux after 2000

The distance that dust of a given size will travel will depend on the fallspeed of the dust, the windspeed, and the height of the dust particles. According to Tegen and Lacis (1996), dust of size 1–10 μm can transport in the atmosphere for only about 40 h. To determine the sources of the dust, we calculated the air-mass distributions arriving at the SE-Dome site from back-trajectory analyses going back three days. The air masses are separated into those from 1000 to 1500 m a.g.l., and those from 10 to 500 m a.g.l. The latter case of the two lower air masses can entrain dust emitted from the surface. Fig. 1 shows these lower air masses. The air masses mainly come from regions of Greenland just north of SE-Dome, extending up to about 75°N, and include regions just offshore as well as some coastal regions to the south. Both periods between 1960–1999 and 2000–2014 have similar distribution patterns of air mass. The similarity suggests that the increase in particle number during 2000–2014 was not driven by a change in atmospheric circulation, but by higher dust emissions in the source regions. Given that the air-mass trajectories do not show the emissions of dust, we focus on specific regions in the higher-probability areas that are likely to have the greatest emissions. These regions would be the snow-free areas in the coastal regions. Thus, we focus on the area marked in red in Fig. 1a.

The area includes the cities of Tasiilaq and Itseqqortoormiit, where the Danish Meteorological Institute (DMI) measures air temperature and precipitation. Tasiilaq is located at a coastal region of southeastern Greenland (~190 km from the SE-Dome site, Fig. 1a). Both annual dust fluxes during 1960–2014 correlate more strongly with air temperature in Tasiilaq (r = 0.61 in Table 3, Fig. 4a) than with that at the SE-Dome site (Table 3). Most coastal regions in southeastern Greenland have exposed snow-free areas of rock, soil, and glacial flour, which are potential dust sources. The lower air masses, which would be the main atmospheric transport for larger dust, come from the eastern coast between 65 and 75 °N of Greenland (Fig. 1). At nearly four times the distance to Tasiilaq lies Itseqqortoormiit (Fig. 1), another potential dust source because it is also on the coast (Fig. 1a). But air temperature in Itseqqortoormiit has lower correlation with the SE-Dome dust (r = 0.35) than that of Tasiilaq. This suggests that the larger dust likely comes from very close to the SE-Dome site.

The autumn dust fluxes during 1960–2014 also have high correlations with autumn air temperature in Tasiilaq (r = 0.50 in Table 3, Fig. 4b). Even omitting the extremely high dust-flux datum from autumn 2014, the autumn average of dust flux (2000–2013) is still highly correlated to the Tasiilaq air temperature (r = 0.52). The correlation suggests that a warmer autumn on the coast increases the dust emission from snow-free areas exposed by a delay of seasonal snowpack. The seasonal snow-free area would be an additional dust source in the coastal regions, especially during autumn. Thus, high correlations between dust flux and Tasiilaq air temperature, both annual and autumn, during 1960–2014 suggest that the warming in the coastal regions of southeastern Greenland after 2000 promotes dust emission to the atmosphere.

The snow-free area trend by AVHRR during 1979–2008 is consistent with such warming, showing a loss of seasonal snowpack in the coastal regions around southeastern Greenland. The snow-free areas of the region in September (Fig. 2c) show an increasing trend after 2000. The average snow-free area in September is 14700 ± 5600 km^2 during 1979–1999 and 21700 ± 10800 km^2 during 2000–2008. This increase suggests that the warmer summers and autumns after 2000 are causing a delay in the seasonal snowpack cover and an extension of snow-free areas. These snow-free areas have high correlation with the autumn dust flux (r = 0.49 for the maximum month, 0.60 for September in Table 3; Fig. 4c). The high correlations suggest a larger snow-free area in autumn increased the dust emission, leading to a higher dust flux in the SE-Dome ice core.

On the other hand, results in Table 3 show low correlations between dust flux and annual Tasiilaq precipitation (r = 0.17) and windspeed (r = 0.41). The Tasiilaq precipitation is a proxy of an aridity in Tasiilaq. Dust is more likely to emit from a source area under drier and windier conditions (e.g., Bullard et al., 2016). The low correlations suggest that the high dust flux after 2000 is not due to a high emission activity of the source area, but rather is due to extend dust emission area (i.e., seasonal snow-free area).

We also examined the correlations between the dust flux and other possible proxy variables. Results in Table 3 show low correlations ($|r| < 0.30$) with the North Atlantic Oscillation (NAO), which is defined as the pressure difference between the Azores High and the Icelandic Low. The low correlations with NAO, as well as the Arctic Oscillation (AO, $|r| < 0.27$) are consistent with the larger dust size distribution during 2000–2014 not being caused by a stronger atmospheric circulation.

Thus, the evidence indicates that the Greenlandic warming produced a larger regional dust emission via a larger seasonal snow-free area in coastal Greenland. The air temperature after 2000 has been increasing throughout the Arctic (Stocker et al., 2013) and specifically around southeastern Greenland (Bjørk et al., 2012), consistent with a retreat of the Greenland ice sheet (Mouginot et al., 2019). As mineral dust plays a key role in the climate system (Carslaw et al., 2010; Kok et al., 2018), the increase in dust flux at the SE-Dome after 2000 is a potentially important way that high-latitude dust can affect the climate system. Future studies about the dynamic of the Greenland ice sheet will need to take into account the role of dust, since increased dust deposition implies an increased radiative forcing on the surface of the ice sheet.

3.4. Contribution of Iceland dust emission

Other than the Greenland coast, the next nearest potential dust source is Iceland. Iceland is also a potential local source of volcanic emissions (Groot Zwaaftink et al., 2017). However, the average air-mass probability distribution from Iceland is just 1.51 ± 1.47% (Fig. 1b and c), which is less than one-third that of the 4.88 ± 2.37% value from 65 to 75 °N of eastern Greenland by the trajectory analyses. Moreover, the fraction of air trajectories from Iceland hardly changes from the earlier period of 1960–1999 (1.53 ± 1.47%) to the recent period of 2000–2014 (1.48 ± 1.49%). Thus, the dust-flux increase after 2000 is not explained by the contribution from Iceland.

Nevertheless, over shorter terms, volcanic eruptions in Iceland have affected dust deposition in the SE-Dome region. For example, the extremely high dust flux in the autumn of 2014 (41.4 mg m^{-2} yr^{-1}) might be due to the eruption of Mt. Bardarbunga in Iceland. However, the contribution of Icelandic volcanic eruptions to dust flux into the SE-Dome ice core should depend on air mass trajectory. Over 1960–2014, seven eruptions in Iceland had a volcanic explosivity index (VEI) exceeding 3 (Table 1). The average number and mass dust concentrations of the term during these seven eruptions are 13700 $\pm$ 8270 ml^{-1} and 40.1 $\pm$ 34.6 μg kg^{-1}, respectively (Table 1). These averages are higher than the overall averages during 1960–2014, but are lower than those during 2000–2014 (Table 1). So, some volcanic events likely contribute to dust deposition in the SE-Dome region (e.g., autumn 2014); however, they cannot explain the increase of dust flux in the SE-Dome ice core after 2000. Baddock et al. (2017) showed similar results. They found that trajectories during Icelandic volcanic seasons rarely ascend high enough to reach inland Greenland, suggesting instead that Icelandic dust has more important effects on the neighboring marine environment than on the cryosphere.

4. Conclusion

We measured particle-size distributions from an ice core in the southeastern dome in Greenland (SE-Dome), using them to reconstruct annual and seasonal dust fluxes during 1960–2014. The annual average flux over the whole period 1960–2014 was 34.8 $\pm$ 13.5 mg m^{-2} yr^{-1}, a value about twice that of inland ice cores. The later term of this period 2000–2014 had the higher annual flux of 46.6 $\pm$ 16.2 mg m^{-2} yr^{-1}. The higher flux, together with other trends, indicated that some dust in the SE-Dome region came from local sources of exposed rock, soil, and sand in coastal Greenland.

The air-mass source locations hardly changed between the terms 1960–1999 and 2000–2014, suggesting that the reason for the larger size distribution during the later term was likely a higher dust production at the source. One nearby coastal source area is Tasiilaq, which had air temperatures that correlated more strongly to the annual and autumn dust fluxes over 1960–2014 than the air temperature in SE-Dome. A probable local source is the region surrounding Tasillaq, where many snow-free areas are found, especially during summer and autumn. In addition, the snow-free area from 65 to 75 °N of southern and eastern Greenland, possible source areas, also was highly correlated during 1979–2008 to the autumn dust flux, especially after 2000. The high dust flux in the SE-Dome ice core after 2000 may indicate a greater influence of high-latitude dust to the future climate system.

Declaration of competing interest

The authors declare that they have no known competing financial interests or personal relationships that could have appeared to influence the work reported in this paper.

Acknowledgements

The authors gratefully acknowledge the Air Resources Laboratory (ARL) for the provision of the HYSPLIT transport and dispersion model on the READY Web site (http://www.arl.noaa.gov/ready.html) and windspeed records at Tasiilaq by National Centers for Environmental Information (NCEI, National Oceanic and Atmospheric Administrationn (NOAA), U. S. (https://www.ncei.noaa.gov/), and acknowledge the Danish Meteorological Institute (DMI), Danmark for the provision of air temperature and precipitation records at Tasiilaq and Itseqqortoormiit. The paper was significantly improved as a result of comments by two reviewers and the handling by Scientific Editor Drs. S. Sandven and M. Fukasawa, to whom we are greatly indebted. We are grateful to the drilling and initial analysis teams of the SE-Dome ice core. This study was supported by MEXT/JSPS KAKENHI Grant Numbers JP18H05292, JP26257201, and JP16H01772, and JP18H03363, and Joint Research Program and the Readership program of the Institute of Low Temperature Science, Hokkaido University. This work was partially carried out in the Arctic Challenge for Sustainability (ArCS and ArCS II) Project, Program Grant Number JPMXD1420318865, and the Environment Research and Technology Development Fund (JPMEERF20202003 and JPMEERF20205001) of the Environmental Restoration and Conservation Agency of Japan. The data used in this study is available in the Hokkaido University Collection of Scholarly and Academic papers (http://hdl.handle.net/2115/79417).

References

Aoki, T., Motoyoshi, H., Kodama, Y., Yasunari, T.J., 2006. Atmospheric aerosol deposition on snow surfaces and its effect on albedo. SOLA 2, 13–16.

Baccolo, G., Delmonte, B., Albani, S., Baroni, C., Cibin, G., Frezzotti, M., Hampai, D., Marcelli, A., Revel, M., Salvatore, M.C., Stenni, B., Maggi, V., 2018. Regionalization of the atmospheric dust cycle on the periphery of the East Antarctic ice sheet since the Last Glacial Maximum. Geochem. Geophys. Geosyst. 19, 3540–3554.

Baddock, M.C., Mockford, T., Bullard, J.E., Thorsteinsson, T., 2017. Pathways of high-latitude dust in the North Atlantic. Earth Planet Sci. Lett. 459 (2017), 170–182.

Biscaye, P., Grousset, F., Revel, M., Van der Gaast, S., Zielinski, G., Vaars, A., Kukla, G., 1997. Asian provenance of glacial dust (stage 2) in the Greenland Ice Sheet Project 2 ice core, Summit, Greenland. J. Geophys. Res. 102 (C12), 26765–26781.

Bjørk, A.A., Kjær, K.H., Korsgaard, N.J., Khan, S.A., Kjeldsen, K.K., Andresen, C.S., Box, J. E., Larsen, N.K., Funder, S., 2012. An aerial view of 80 years of climate related glacier fluctuations in southeast Greenland. Nat. Geosci. 5, 427–432. https://doi.org/10.1038/NGEO1481.

Bory, A.J.-M., Biscaye, P.E., Piotrowski, A.M., Steffensen, J.P., 2003. Regional variability of ice core dust composition and provenance in Greenland. Geochem. Geophys. Geosyst 4 (12), 1107. https://doi.org/10.1029/2003GC000627.

Bory, A.J.-M., Biscaye, P.E., Svensson, A., Grousset, F.E., 2002. Seasonal variability in the origin of recent atmospheric mineral dust at NorthGRIP, Greenland. Earth Planet Sci. Lett. 196 (3–4), 123–134.

Bullard, J.E., 2013. Contemporary glacigenic inputs to the dust cycle. Earth Surf. Process. Landforms 38, 71–89. https://doi.org/10.1002/esp.3315.

Bullard, J.E., Baddock, M., Bradwell, T., Crusius, J., Darlington, E., Gaiero, D., Gasso, S., Gisladottir, G., Hodgkins, R., McCulloch, R., McKenna-Neuman, C., Mockford, T., Stewart, H., Thorsteinsson, T., 2016. High-latitude dust in the Earth system. Rev. Geophys. 54, 447–485.

Greenland-DMI historical climate data collection 1784-2015. In: Cappelen, J. (Ed.), DMI Tech. Rep 16–04. https://www.dmi.dk/fileadmin/user_upload/Rapporter/TR/2016/DMIRep16-04.pdf.

Carslaw, K.S., Boucher, O., Spracklen, D.V., Mann, G.W., Rae, J.G.L., Woodward, S., Kulmala, M., 2010. A review of natural aerosol interactions and feedbacks within the Earth system. Atmos. Chem. Phys. 10, 1701–1737.

Dee, D.P., Uppala, S.M., Simmons, A.J., Berrisford, P., Poli, P., Kobayashi, S., Andrae, U., Balmaseda, M.A., Balsamo, G., Bauer, P., Bechtold, P., Beljaars, A.C.M., Van de Berg, L., Bidlot, J., Bormann, N., Delsol, C., Dragani, R., Fuentes, M., Geer, A.J., Haimberger, L., Healy, S.B., Hersbach, H., Hólm, E.V., Isaksen, L., Kållberg, P., Köhler, M., Matricardi, M., McNally, A.P., Monge-Sanz, B.M., Morcrette, J.-J., Park, B.-K., Peubey, C., de Rosnay, P., Tavolato, C., Thépaut, J.-N., Vitart, F., 2011. The ERA-Interim reanalysis: configuration and performance of the data assimilation system. Q. J. Roy. Meteorol. Soc. 137, 553–597. https://doi.org/10.1002/qj.828.

Delmonte, B., Andersson, P., Hansson, M., Schoberg, H., Petit, J.-R., Basile-Doelsch, I., Maggi, V., 2008. Aeolian dust in East Antarctica (EPICA-Dome C and Vostok): provenance during glacial ages over the last 800 kyr. Geophys. Res. Lett. 35, L07703 https://doi.org/10.1029/2008GL033382.

DiMarzio, J.P., GLAS/ICESat 1 km Laser Altimetry Digital Elevation Model of Greenland, Version 1. Boulder, Colorado USA. NSIDC: National Snow Ice Data Center. https://doi.org/10.5067/FYMKT3GJE0TM.

Fujita, K., 2007. Effect of dust event timing on glacier runoff: sensitivity analysis for a Tibetan glacier. Hydrol. Process. 21 (21), 2892–2896. https://doi.org/10.1002/hyp.6504.

Fujita, K., Takeuchi, N., Nikitin, S.A., Surazakov, A.B., Okamoto, S., Aizen, V.B., Kubota, J., 2011. Favorable climatic regime for maintaining the present-day geometry of the Gregoriev Glacier, Inner Tien Shan. Cryosphere 5 (3), 539–549. https://doi.org/10.5194/tc-5-539-2011.

Furukawa, R., Uemura, R., Fujita, K., Sjolte, J., Yoshimura, K., Matoba, S., Iizuka, Y., 2017. Seasonal scale dating of shallow ice core from Greenland using oxygen isotope matching between data and simulation. J. Geophys. Res. Atmos. 122 https://doi.org/10.1002/2017JD026716.

Groot Zwaaftink, C.D., Arnalds, O., Dagsson-Waldhauserova, P., Eckhardt, S., Prospero, J.M., Stohl, A., 2017. Temporal and spatial variability of Icelandic dust emissions and atmospheric transport. Atmos. Chem. Phys. 17, 10865–10878. https://doi.org/10.5194/acp-17-10865-2017.

Higgins, R.W., Zhou, Y., Kim, H.-K., 2001. Relationships between el niño-southern oscillation and the Arctic oscillation: a climate-weather link. NCEP/Climate Predi. Center ATLAS 8.

Hori, M., Sugiura, K., Kobayashi, K., Aoki, T., Tanikawa, T., Kuchiki, K., Niwano, M., Enomoto, H., 2017. A 38-year (1978–2015) Northern Hemisphere daily snow cover extent product derived using consistent objective criteria from satellite-borne optical sensors. Remote Sens. Environ. 191, 402–418. https://doi.org/10.1016/j.rse.2017.01.023.

Hurrell, J.W., Kushnir, Y., Ottersen, G., Visbeck, M., 2003. An overview of the North Atlantic oscillation. In: The North Atlantic Oscillation: Climate Significance and Environmental Impact, Geophys. Monogr, vol. 134. Amer. Geophys. Union, pp. 1–35. https://doi.org/10.1029/134GM01.

Iizuka, Y., Miyamoto, A., Hori, A., Matoba, S., Furukawa, R., Saito, T., Fujita, S., Hirabayashi, M., Yamaguchi, S., Fujita, K., Takeuchi, N., 2017. A firn densification process in the high accumulation dome of southeastern Greenland. Arctic Antarct. Alpine Res. 49, 13–27.

Iizuka, Y., Uemura, R., Fujita, K., Hattori, S., Seki, O., Miyamoto, C., Suzuki, T., Yoshida, N., Motoyama, H., Matoba, S., 2018. A 60 year record of atmospheric aerosol depositions preserved in a high accumulation dome ice core, Southeast Greenland. J. Geophys. Res.: Atmosphere 123. https://doi.org/10.1002/2017JD026733.

Iizuka, Y., Miyake, T., Hirabayashi, M., Suzuki, T., Matoba, S., Motoyama, H., Fujii, Y., Hondoh, T., 2009. Constituent elements of insoluble and nonvolatile particles during the Last Glacial Maximum of the Dome Fuji ice core. J. Glaciol. 55 (191), 552–562.

Kok, J.F., Ward, D.S., Mahowald, N.M., Evan, A.T., 2018. Global and regional importance of the direct dust-climate feedback. Nat. Commun. 9, 241.

Lambert, F., Delmonte, B., Petit, J.R., Bigler, M., Kaufmann, P.R., Hutterli, M.A., Stocker, T.F., Ruth, U., Steffensen, J.P., Maggi, V., 2008. Dust–climate couplings over the past 800,000 years from the EPICA Dome C ice core. Nature 452, 616–619.

Liu, J. D. Wu, Liu, G., Mao, R., Chen, S., Ji, M., Fu, P., Sun, Y., Pan, X., Jin, H., Zhou, Y., Wang, X., 2020. Impact of Arctic amplification on declining spring dust events in East Asia. Clim. Dynam. 54, 1913–1935. https://doi.org/10.1007/s00382-019-05094-4.

Mahowald, N., Muhs, D., Levis, S., Rasch, P., Yoshioka, M., Zender, C., 2006. Change in atmospheric mineral aerosols in response to climate: last glacial period, preindustrial, modern, and doubled carbon dioxide climates. J. Geophys. Res. 111, D10202.

Mahowald, N., Albani, S., Kok, J.F., Engelstaeder, S., Scanza, R., Ward, D.S., Flanner, M. G., 2014. The size distribution of desert dust aerosols and its impact on the Earth system. Aeolian Res. 15, 53–71.

Mouginot, J., Rignot, E., Bjørk, A.A., Van den Broeke, M., Millan, R., Morlighem, M., Noël, B., Scheuchl, B., Wood, M., 2019. Forty-six years of Greenland Ice Sheet mass balance from 1972 to 2018. Proc. Natl. Acad. Sci. Unit. States Am. 116 (19), 9239–9244.

Nagorski, S.A., Kaspari, S.D., Hood, E., Fellman, J.B., Skiles, S.M., 2019. Radiative forcing by dust and black carbon on the juneau Icefield. Alaska 124, 3943–3959. https://doi.org/10.1029/2018JD029411.

Sakai, A., Nuimura, T., Fujita, K., Takenaka, S., Nagai, H., Lamsal, D., 2015. Climate regime of Asian glaciers revealed by GAMDAM glacier inventory. Cryosphere 9, 865–880. https://doi.org/10.5194/tc-9-865-2015.

Saros, J.E., Anderson, N.J., Juggins, S., McGowan, Yde, J.C., Telling, J., Bullard, J.E., Yallop, M.L., Heathcote, A.J., Burpee, B.T., Fowler, R.A., Barry, C.D., Northington, R. M., Osburn, C.L., Pla-Rabes, S., Mernild, S.H., Whiteford, E.J., Andrews, M.G., Kerby, J.T., Post, E., 2019. Arctic climate shifts drive rapid ecosystem responses across the West Greenland landscape. Environ. Res. Lett. 14 (2019), 074027.

Seinfeld, J.H., Pandis, S.N., 1998. Atmospheric Chemistry and Physics: from Air Pollution to Climate Change. John Wiley & Sons Inc., New York.

Simonsen, M.F., Baccolo, G., Blunier, T., Borunda, A., Delmonte, B., Frei, R., Goldstein, S., Grinsted, A., Kjær, H.A., Sowers, T., Svensson, A., Vinther, B., Vladimirova, D., Winckler, G., Winstrup, M., Vallelonga, P., 2019. East Greenland ice core dust record reveals timing of Greenland ice sheet advance and retreat. Nat. Commun. 10, 4494. https://doi.org/10.1038/s41467-019-12546-2.

Stanelle, T., Bey, I., Raddatz, T., Reick, C., Tegen, I., 2014. Anthropogenically induced changes in twentieth century mineral dust burden and the associated impact on radiative forcing. J. Geophys. Res. Atmos. 119, 13526–13546.

Stein, A.F., Draxler, R.R., Rolph, G.D., Stunder, B.J.B., Cohen, M.D., Ngan, F., 2015. NOAA's HYSPLIT atmospheric transport and dispersion modeling system. Bull. Am. Meteorol. Soc. 96 (12), 2059–2077. https://doi.org/10.1175/BAMS-D-14-00110.1.

Stocker, T.F., Qin, D., Plattner, G.-K., Tignor, M., Allen, S.K., Boschung, J., Nauels, A., Xia, Y., Bex, V., Midgley, P.M. (Eds.), 2013. Climate Change 2013: the Physical Science Basis. Contribution of Working Group I to the Fifth Assessment Report of the Intergovernmental Panel on Climate Change. Cambridge University Press, Cambridge, United Kingdom and New York, NY, USA, p. 1535. https://doi.org/10.1017/CBO9781107415324.

Tegen, I., Lacis, A.A., 1996. Modeling of particle size distribution and its influence on the radiative properties of mineral dust aerosol. J. Geophys. Res. 101, 19237–19244.

Tobo, Y., Adachi, K., DeMott, P.J., Hill, T.C.J., Hamilton, D.S., Mahowald, N.M., Nagatsuka, N., Ohata, S., Uetake, J., Kondo, Y., Koike, M., 2019. Glacially sourced dust as a potentially significant source of ice nucleating particles. Nat. Geosci. 12, 253–258. https://doi.org/10.1038/s41561-019-0314-x.

Uno, I., Eguchi, K., Yumimoto, K., Takemura, T., Shimizu, A., Uematsu, M., Liu, Z., Wang, Z., Hara, Y., Sugimoto, N., 2009. Asian dust transported one full circuit around the globe. Nat. Geosci. 2 (8), 557–560.

Uppala, S.M., Kållberg, P.W., Simmons, A.J., Andrae, U., Da Costa Bechtold, V., Fiorino, M., Gibson, J.K., Haseler, J., Hernandez, A., Kelly, G.A., Li, X., Onogi, K., Saarinen, S., Sokka, N., Allan, R.P., Andersson, E., Arpe, K., Balmaseda, M.A., Beljaars, A.C.M., Van De Berg, L., Bidlot, J., Bormann, N., Caires, S., Chevallier, F., Dethof, A., Dragosavac, M., Fisher, M., Fuentes, M., Hagemann, S., Hólm, E., Hoskins, B.J., Isaksen, L., Janssen, P.A.E.M., Jenne, R., McNally, A.P., Mahfouf, J.F., Morcrette, J.-J., Rayner, N.A., Saunders, R.W., Simon, P., Sterl, A., Trenberth, K.E., Untch, A., Vasiljevic, D., Viterbo, P., Woollen, J., 2005. The ERA-40 re-analysis. Q. J. R. Meteorol. Soc. 131, 2961–3012.